# An Acoustic On-Chip Goniometer for Room Temperature Macromolecular Crystallography

C. G. Burton,[a] D. Axford,[b] A.M.J. Edwards,[c] R. Gildea,[b] R.H. Morris,[c] M. I. Newton,[c] A.M.Orville, [d] M.Prince,[a] P.D.Topham,[a] and P.D.Docker, [b]†

**This paper describes the design, development and succesful use of an on-chip goniometer for room-temperature macromolecular crystallography via acoustically induced rotations. We present for the first time a low cost, rate-tunable, acoustic actuator for** for gradual in-fluid sample reorientation about varying axes **and its utilisation for protein structure determination on a synchrotron beamline. The device enables the efficient collection of diffraction data *via* a rotation method from a sample within a surface confined droplet. This method facillitates efficient macromolecular structural data acquisition in fluid environments for dynamical studies.**

Lab-on-a-Chip technology provides significant advantage in handling microparticle suspensions. High throughput sorting, chemical treatment and analysis become possible because of dramatic system simplification. Advances in detector technology and X-ray optics means synchrotron based macromolecular crystallography (MX) can now take advantage of new methodologies such as Lab-on-a-chip. MX has an experimental pipeline that relies on the coordination of many complex, precision processes both human and mechanical. Processes that typically culminate with a single crystal isolated by hand on to a standard loop, representing considerable researcher effort. In recent years a diverse set of techniques have been developed for increased throughput in MX crystal handling, including: hydrodynamic traps, high density grid mounting, graphene microfluidics and acoustic levitation to name but a few.[1–6] In order to determine the structure of a macromolecule by X-ray crystallography a complete set of the specifically oriented scattered beams (reflections) needs to be captured by a two-dimensional detector. Traditionally this is achieved by orienting and rotating the sample with a mechanical goniometer however serial methods, pioneered at X-ray Free Electron Laser (XFEL) sources, rely instead on collecting a single detector image from a large number (1000s) of randomly oriented crystals.[7] As such XFEL sample presentation methods are typically much more dynamic, and include injectors that encompass gas virtual dynamic nozzles, lipidic cubic phase (LCP) extruders, acoustic droplet ejection (ADE), or concentric-flow electrokinetic injectors.[8–12] Alternatively, fixed target sample delivery methods include ADE coupled with a conveyor belt and various types of fixed targets wherein stationary samples are brought rapidly to the interaction region.[10,13] All of these room temperature methods avoid structural artefacts that may be induced on cryogenic cooling and in certain cases samples, such as viruses, can suffer significant degradation in crystal quality when cryo-cooled.[14,15]

Our approach utilises a surface acoustic wave transducer to generate chaotic rotation of crystals within a fluid environment during X-ray diffraction.[16] The approach occupies a uniquely small footprint and is able to maximise the amount of data from individual crystals, particularly with respect to serial methods, reducing the amount of sample required for structure elucidation.[8] Device specification was driven by the need for room temperature operation, ensuring the opportunity to resolve dynamic protein elements. Further as there is no need to mount the crystal, nor remove it from precipitation solution, the induced rotation resolves a key challenge, namely >90° crystal rotation in microfluidic and crystallisation tray based diffraction. As such the method is able to maximise the amount

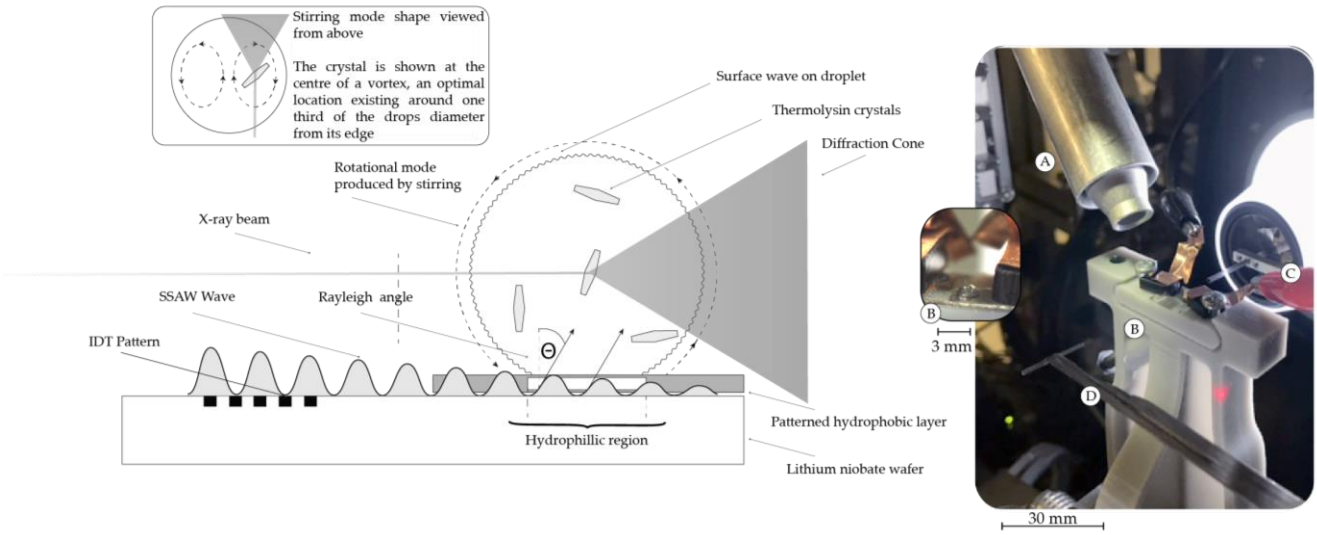


Figure 1 A schematic of the stirring mechanism used to actuate the protein crystals in precipitation solution. The surface wave can be seen to refract energy in to the drop at the Rayleigh angle. The beam arrives from behind the sample, meeting a crystal and diffracting in to a cone of around 0.7 steradians. The hydrophilic / hydrophobic patterning can be seen on the substrate beneath the drop in the schematic. In the right hand image the HC1 controller nozzle (A), the device on a grey kinematic mount (B). The beam arrives along the axis of the optics (C) and scattered X-rays exit past the beam stop (D) to the detector (out of view to the left). A CAD model of the goniometer mount is included in supporting information ESI 1

of data from individual crystals particularly with respect to serial methods, reducing the amount of sample required for structure elucidation. Acoustic handling was demonstrated to be safe for several types of protein crystal by Guo et al, in a work where crystals were acoustically trapped and then sent for later X-ray diffraction analysis.[17]

The following work describes the hand mounting of a single drop containing traditionally sized protein crystals (>100 µm) on to a surface acoustic wave device. The device is used to actuate the crystals, one of which is trapped and imaged at the centre of a 'low speed vortex'. We demonstrate the successful imaging of a crystal under acoustic excitation, the potential of vortex entrapment for high throughput microfluidic crystallography techniques and successful data processing for structure determination despite the limitations of existing methods made apparent.

## Methodology

The standing surface acoustic wave (SSAW) actuation system is comprised of a 3D printed kinematic 'chip' and a fixed mount, a piezo electric wafer section and a patterned hydrophobic layer for fluid deposition. Generation of a surface wave was achieved through patterned titanium and gold interdigitated electrodes (IDT) excited by a pulsed

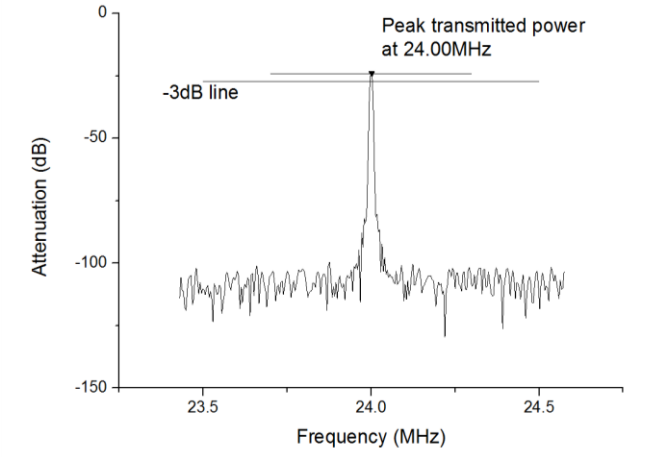


Figure 2 Frequency response of the SSAW device after the wave has traversed the region containing the drop. The wave power was received by a secondary SSAW device incorporated into the mask design for this purpose. The -3dB line shows the point at which power transmission has dropped by 50% indicating a sharp resonance.

sine wave of 24 MHz and 50% duty cycle which was further cycled on and off at 1 Hz.[18,19] To form the IDT titanium was sputter coated to form an adherent layer on the surface of the lithium niobate. This was then coated with gold to form an electrically conductive layer. A photolithographic 'lift off' process produced a periodic structure of an IDT on the surface of 128° rotated y cut, x propagating $LiNbO_3$.

The fabrication used S1813 (Microposit, Dow), and a chrome mask from (JD Photo Data, UK). The transducer was designed as a single-single type, with periodicity set to 160 µm. To excite the SSAW device, a signal generator (DSG4102, Rigol) was coupled to an amplifier (Henry Radio 20B, USA). The velocity of the samples within the drop were controlled by amplitude of the signal waveform, with pulse duty cycle being used to limit the power added to the device. The waveform can be described as a 24 MHz 50% duty cycle pulsed sine wave, additionally globally cycled at 1 s intervals. Velocity was calculated by digital image correlation.

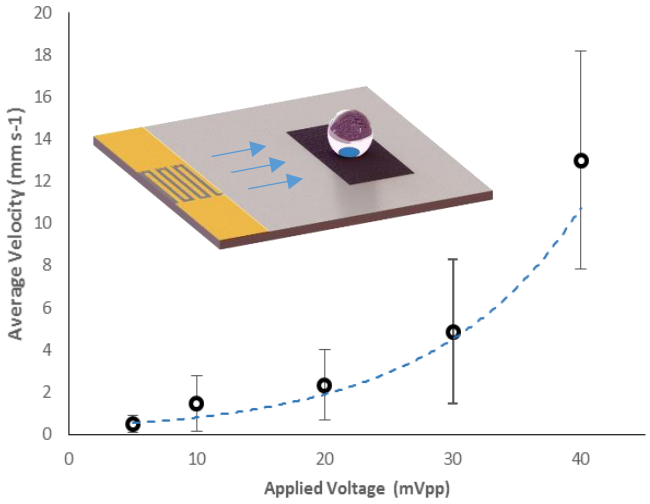


Figure 3 Velocity of the crystals in solution once the SSAW wave is applied. Error bars indicate standard deviation of measurements, and voltage level is shown pre amplification. Voltage level and mean velocity were correlated approximately exponentially, this trend is indicated by the dashed line. Measurements were taken using digital image correlation using telecentric imaging apparatus. Overlay shows illustrative view of an IDT, with the arrow showing direction of propagation for the SSAW wave. The hydrophobic locating pattern is shown in black and the hydrophilic locating spot shown in blue beneath the fluid drop

| Data collection | |
|---|---|
| Exposure Time (ms) | 10 |
| Beam size (µm) | 50 x 50 |
| Wavelength (Å) | 0.9686 |
| Incident flux (photons $s^{-1}$) | 6 x $10^{11}$ |
| No. integrated frames | 2796 |
| No. scaled & merged frames | 2670 |
| **Scaling** | |
| Space group | $P6_122$ |
| Unit cell parameters (Å) | 93.6, 93.6, 129.8 |
| Resolution range (Å) | 44.0 – 2.0 (2.2 – 2.0) |
| $R_{split}$ | 0.092 (1.038) |
| $CC_{1/2}$ | 0.993 (0.290) |
| $(I/\sigma(I))$ | 2.19 (0.19) |
| Multiplicity | 61.20 (42.1) |
| Completeness (%) | 99.2 (99.8) |
| **Refinement** | |
| No. reflections | 26888 |
| No. non-H atoms (Protein) | 2480 |
| No. non-H atoms (Water) | 108 |
| $R/R_{free}$ | 0.201/0.256 |
| R.m.s.d, bond lengths (Å) | 0.010 |
| R.m.s.d., bond angles (°) | 1.11 |
| Ramachandran outliers (%) | 0 |
| Side chain outliers (%) | 0.8 |
| PDB code | 5O8N |

Table 1. Summary statistics for diffraction data processing and refinement.

The hydrophobic surface was fabricated by Scientific Device Laboratory (Scientific Device Laboratory, USA), an inkjet printed fluorinated ink was selectively patterned onto a Kapton substrate. The pattern was a solid block of colour except for a small hydrophilic dot in the centre designed to locate the crystal laden drop, see overlay in Figure 3. The material was fixed using ethyl cyanoacrylate glue (Loctite 401) to enable effective transmission of the surface wave through and into the film and fluid. Measured sessile water drop contact angle for a located drop was 84°, compared to 64° for Kapton Hn (Cole-Parmer, UK) alone, illustrating its more hydrophobic character.

**Thermal Characterisation**

Infrared measurements were taken to evaluate the heating experienced by the 2 µl drop during stirring using a Fluke Ti400 on a fixed mount over a period of 1 minute without the assistance of external cooling. This is comparable with the length of time a single drop was exposed to the X-ray beam and SSAW stirring. A video is included in supporting information (ESI 4).

**Sample preparation**

Commercial thermolysin from Bacillus thermoproteolyticus (Sigma-Aldrich) was resuspended to a concentration of 50 mg $ml^{-1}$ in a solution of 45% dimethyl sulfoxide, 0.5 M NaCl and 50 mM 2-(N-morphlino)ethanesulfonic acid (MES buffer) to a

pH of 6.0. Sitting drops were made by mixing 2 µl protein solution and 2 µl reservoir solution, consisting of 1.2 M ammonium sulfate in 18.2 MΩ water, and equilibrated against 300 µl of this reservoir solution at 20 °C in sealed trays. Crystals approximately 50 x 50 x 200 µm in dimension grew within 7 days. Immediately prior to data collection 2 µl of a sitting drop containing multiple crystals was manually transferred by pipette to the chip surface.

**Synchrotron data collection**

The experiments took place at beamline i24 at the Diamond Light Source, Harwell, Oxford. The X-ray beam was defocused to 50 $\mu m^2$ to best match the dimensions of the crystal within the 2 µl drop (1800-2500 µm diameter dependent intersection point of the beam with the drop). Diffraction data were recorded with a Pilatus3 6M operating at its maximum frame rate of 100 Hz. Guided by an on X-ray beam axis camera, the chip was aligned to the beam using the high-precision piezo-electric sample positioning stages. The optimised interaction point was found to be approximately consistent with the 'sweet spot' in Figure 1, central to the droplet at a height of approximately 3/4 of the total drop to limit shadowing on the lower half of the detector from the edge of the chip.

To prevent the sample containing droplet from evaporating in the dry air of the beamline (ambient humidity recorded at 17% by portable device) the HC1 sample humidity control device was used.[20] This provided a constant flow of 96% humidity air over the drop at 293 K, it is important to note that no contribution to sample motion was observed from the airflow. A number of collection 'runs' were performed typically lasting 50 seconds and recording 5000 images.

**Diffraction data processing**

Detector images with diffraction data were analysed with the DIALS software package using the specific routine dials.stills_process to perform diffraction spot finding, space group and unit cell indexing, determination of the crystal rotation matrix, and reflection integration.[21] Individual integration files were merged and put on a common scale using the program PRIME.[22] An example detector image is included in the supporting information (ESI 2).

**Structure solution**

The crystal structure was solved using molecular replacement with protein data bank (pdb) entry 5UU9 truncated to polyalanine. Model building was completed using Phenix autobuild and Coot and refinement was performed with Phenix refine. Statistics for data collection and refinement are presented in Table 1.

## Results and Discussion

The SSAW transducer was designed to achieve a resonant frequency of 24 MHz which gave a short wavelength while allowing for a high device yield during production. The sharp frequency response of the device can be seen in Figure 2 where the -3dB bandwidth was 0.02 MHz (the point that corresponds to a 50% received signal power reduction). Off beam trials showed that after 30s of SSAW actuation no significant droplet reduction occurred *via* evaporation or ejection. The switching pattern was determined through observation, of the inertia of the moving crystals and fluid needed, to maintain sufficient rotation.

Results of thermal imaging showed that the drop experienced a heating rate of approximately 42 mJ $s^{-1}$. In context the heating rate was equivalent to 0.1 $ks^{-1}$, with both the drop and piezo temperature benefitting from reduced heating due to the waveform described above (supplementary information figure ESI 4).

Crystal translation during operation was monitored using custom telecentric video imaging arrangement giving optimal depth of field. The arrangement made use of various mountings to achieve a birds-eye view of the drop, and a 1.7x high resolution lens for optimised depth of field and resolution (#63-232, Edmund Optic UK). The motion of crystals within the drop ranged between gentle rocking of a crystal (mimicking the small rotation method of a goniometer) to greater than 15 000 µm $s^{-1}$ at high signal amplitudes, which is markedly faster than current detector frame rates and gave rise to increase in drop heating.

The widening velocity ranges in Figure 3 is due to the centre and the edge of a rotating system having different velocities. This implies a vortex or other complex rotation is induced by the SSAW interacting with the drop. Differences in translational velocity between the drop centre and edge naturally increased with rotational speed. During diffraction SSAW power was applied to achieve an actuation speed range of approximately 0-800 µm $s^{-1}$ in the xy plane. This velocity implies a single crystal within a multi crystal drop could intersect the beam for between

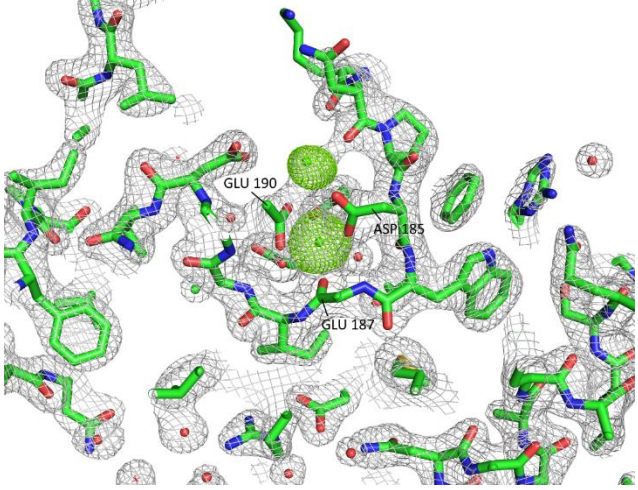


Figure 4 Example of electron density to 2.0 Å resolution around the thermolysin model 5ON8. In this case the occupancy of two calcium atoms has been set to zero and a 2Fo-Fc map is shown (contoured at 1 σ) and a Fo-Fc difference map (contoured to 5σ) which highlights these atom sites in green, indicating scattering in the data not accounted for in the reduced occupancy model.

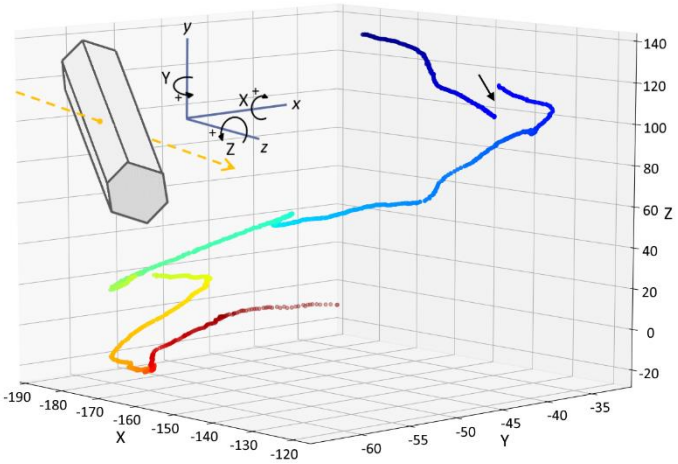


Figure 5 A 3 dimension scatter plot of Euler x,y,z rotation angles (in degrees) derived from the orientation matrix from 1709 diffraction images across which a consistent and unambiguous indexing solution could be tracked, thus illustrating the motion of the sample. The colour map indicates the sequence of observations from blue to red. The in-laid schematic describes the beamline coordinate system with the X-ray beam (dashed arrow) along the Z axis and the angles X,Y,Z representing rotations about the respective *x,y,z* axes. The black arrow indicates a gap where the crystal briefly moved out of the beam. An animation of the rotation is included in supplementary information ESI 5

6 and 25 detector frames (at 100 Hz) with the full crystal while in pure translation, however in the instances when the crystal arrives at the centre of a vortex within the drop, the crystal may be imaged in a stream of consecutive frames, as illustrated by the tracking of incremental changes in the rotation matrix for each processed diffraction image. A video showing stirring motion is included in the supporting information ESI 3. On the beamline, highest 'hit-rates', i.e. diffraction data recorded on consecutive images, were found with the beam part way across the drop and consistent with the schematic in Figure 1. When the beam passed close to the edge of a drop diffraction hits were inconsistent, deduced to be crystals translating across the beam as they orbited the droplet (plots can be seen in ESI 6).

Whilst acoustic sample manipulation has seen prior application *via* a levitating droplet, we use a surface-based method, compatible with a continuous microfluidic on-chip device, with the potential for high sample throughput and initiation of enzyme reactions for dynamic studies.[17,23] In comparison to more conventional microfluidic sample handling systems, acoustically induced sample orientation enabled the acquisition of a complete set of reflections without the need to move the device itself.[24,25]

The thermolysin crystal structure (Structure factors and coordinates have been deposited under pdb entry 5O8N) was determined from a collection run of 5000 images, 2670 of which made up the final dataset, and statistics are presented in Table 1. The dataset is from a single drop and likely from a single crystal however there is a gap of ~200 frames within the block of useful images where no diffraction is seen and the possibility of an exchange of crystals at this point cannot be completely ruled out. The DIALS software suite allows multiple crystal lattices to be identified and deconvolved[26]. Plot 8 in ESI illustrates how most images for this collection run contained a single lattice. A number of smaller clusters of images contained a second lattice and a few images showed a third recordable lattice. This observation supports the model of a central crystal spinning on the spot with other crystals orbiting and hence only appearing transiently in the beam. An example of electron density from the refined structure is provided in Figure 4. Using Raddose-3D and assuming a single crystal consistently illuminated, average diffraction weighted X-ray dose was calculated at 0.6 M Gy.[27] This is of the order of the maximum dose from which useful diffraction data can be collected at room temperature and there was no obvious drop in diffracting power seen in the later diffraction images.[28] The data confirms the device's ability to produce useful structures from acoustically perturbed µl volumes, without moving parts or crystal mounting. The dataset reflects a crystal captured at the centre of the vortex and rotating relatively slowly (see supplementary animation video X). Processing *via* a serial method assumes each detector frame to be an individual experiment and refines an independent crystal lattice orientation for each instance. Refined crystal lattice orientation for adjacent detector frames with consistent indexing from the dataset is plotted in Figure 5. The continuous line indicates a single lattice is being tracked and the plot displays the motion of the crystal during the data collection. A break in the line (arrow) indicates where the crystal has temporarily moved out of the beam. The predominant motion is a ~180° rotation about the *z* axis (beam axis) accompanied by ~60° about the *x* axis (horizontal) and ~35° about the *y* axis (vertical). The speed of rotation can be seen to vary during the collection. The plot represents a time series of ~17 s equating to an average rotation speed about the dominant axis of ~10°$s^{-1}$ or ~0.1° per detector frame. The ability to measure a complete set of crystal reflections is most likely enhanced by the fact that rotation of the crystal is not about a single fixed axis.

However, there is currently no software able to properly handle such a goniometer-based experiment. Therefore in this case we have turned to serial crystallography methods to analyse detector frames on an individual basis. We are currently developing routines to correctly model the varying motion of the sample from frame to frame with the expectation of improving data analysis from this type of experiment. In addition to thermolysin, a small, time-limited amount of diffraction data were collected on thaumatin crystals but are not presented here. These findings suggested, with a similar amount of effort, comparable results would be obtained with thaumatin, demonstrating the potential of the method in differing fluid conditions. In the case of thaumatin these conditions were 0.05M (acetamido)iminodiacetic acid, pH 6.8, 0.6M Potassium/sodium tartrate and 20% glycerol.

## Conclusions

Our on-chip crystal rotation method enables efficient room temperature in situ X-ray data collection of protein crystals without the need for multi-axis goniometry and complex precision motion systems. The diffraction data acquired from the device are of good quality, despite a sub-optimal X-ray background and scattering cone. Data analysis was facilitated with the collection of rotation images rather than the still measurements obtained from most serial crystallography methods which consist only of partial reflections. The wide range of speed control achieved by varying input power allowed sample translation and rotation at speeds appropriate to the 1ms detector read out time, boosting data collection efficiency and quality. Precise X-ray dose quantification for the experiment is difficult since the relatively unconstrained motion of the sample is likely to be bringing fresh sample volume in and out of the beam. Although crystal diffracting power was not seen to dramatically decline over the dataset, the chance of radiation induced changes should always be anticipated at room temperature. Going forward, we plan the incorporation of microfluidics into the experimental design. A full Lab-on-a-Chip system is envisioned, moving towards automated sample delivery without the need for costly and complex robotics or time consuming user mounting. A sealed environment would be a valuable addition, preventing liquid loss *via* evaporation and removing the need for humidity control. In summary this technique has been proven for the first time to meet the demanding needs of macromolecular protein crystallography, and by achieving a high resolution structure the device makes a significant stride in automating sample handling.

## Conflicts of Interest

There are no conflicts to declare.

## Acknowledgements

The authors thank James Duggins, Tracey Keates, and Darren Sherrell, for their technical assistance and Diamond Light Source for funding. A.M.O acknowledges support from a Strategic Award from the Wellcome Trust and the Biotechnology and Biological Sciences Research Council (grant 102593).

## Notes and references

1 A. Otten, S. Köster, B. Struth, A. Snigirev and T. Pfohl, *J. Synchrotron Radiat.*, 2005, **12**, 745–750.

2 A. Marmur, *Langmuir*, 2003, **19**, 8343–8348.

3 A. Le Maire, M. Gelin, S. Pochet, F. Hoh, M. Pirocchi, J. F. Guichou, J. L. Ferrer and G. Labesse, *Acta Crystallogr. Sect. D Biol. Crystallogr.*, 2011, **67**, 747–755.

4 K. Dhouib, C. Khan Malek, W. Pfleging, B. Gauthier-Manuel, R. Duffait, G. Thuillier, R. Ferrigno, L. Jacquamet, J. Ohana, J.-L. Ferrer, A. Théobald-Dietrich, R. Giegé, B. Lorber and C. Sauter, *Lab Chip*, 2009, **9**, 1412–1421.

5 C. A. Smith and A. E. Cohen, *JALA - J. Assoc. Lab. Autom.*, 2008, **13**, 335–343.

6 S. Sui, Y. Wang, K. W. Kolewe, V. Srajer, R. Henning, J. D. Schiffman, C. Dimitrakopoulos and S. L. Perry, *Lab Chip*, 2016, **16**, 3082–3096.

7 H. N. Chapman, P. Fromme, A. Barty, T. A. White, R. A. Kirian, A. Aquila, M. S. Hunter, J. Schulz, D. P. DePonte, U. Weierstall, R. B. Doak, F. R. N. C. Maia, A. V. Martin, I. Schlichting, L. Lomb, N. Coppola, R. L. Shoeman, S. W. Epp, R. Hartmann, D. Rolles, A. Rudenko, L. Foucar, N. Kimmel, G. Weidenspointner, P. Holl, M. Liang, M. Barthelmess, C. Caleman, S. Boutet, M. J. Bogan, J. Krzywinski, C. Bostedt, S. Bajt, L. Gumprecht, B. Rudek, B. Erk, C. Schmidt, A. Hömke, C. Reich, D. Pietschner, L. Strüder, G. Hauser, H. Gorke, J. Ullrich, S. Herrmann, G. Schaller, F. Schopper, H. Soltau, K.-U. Kühnel, M. Messerschmidt, J. D. Bozek, S. P. Hau-Riege, M. Frank, C. Y. Hampton, R. G. Sierra, D. Starodub, G. J. Williams, J. Hajdu, N. Timneanu, M. M. Seibert, J. Andreasson, A. Rocker, O. Jönsson, M. Svenda, S.

Stern, K. Nass, R. Andritschke, C.-D. Schröter, F. Krasniqi, M. Bott, K. E. Schmidt, X. Wang, I. Grotjohann, J. M. Holton, T. R. M. Barends, R. Neutze, S. Marchesini, R. Fromme, S. Schorb, D. Rupp, M. Adolph, T. Gorkhover, I. Andersson, H. Hirsemann, G. Potdevin, H. Graafsma, B. Nilsson and J. C. H. Spence, *Nature*, 2011, **470**, 73–77.

8 D. P. DePonte, U. Weierstall, K. Schmidt, J. Warner, D. Starodub, J. C. H. Spence and R. B. Doak, *J. Phys. D. Appl. Phys.*, 2008, **41**, 195505.

9 R. G. Sierra, H. Laksmono, J. Kern, R. Tran, J. Hattne, R. Alonso-Mori, B. Lassalle-Kaiser, C. Gl??ckner, J. Hellmich, D. W. Schafer, N. Echols, R. J. Gildea, R. W. Grosse-Kunstleve, J. Sellberg, T. A. McQueen, A. R. Fry, M. M. Messerschmidt, A. Miahnahri, M. M. Seibert, C. Y. Hampton, D. Starodub, N. D. Loh, D. Sokaras, T. C. Weng, P. H. Zwart, P. Glatzel, D. Milathianaki, W. E. White, P. D. Adams, G. J. Williams, S. Boutet, A. Zouni, J. Messinger, N. K. Sauter, U. Bergmann, J. Yano, V. K. Yachandra and M. J. Bogan, *Acta Crystallogr. Sect. D Biol. Crystallogr.*, 2012, **68**, 1584–1587.

10 C. G. Roessler, R. Agarwal, M. Allaire, R. Alonso-Mori, B. Andi, J. F. R. Bachega, M. Bommer, A. S. Brewster, M. C. Browne, R. Chatterjee, E. Cho, A. E. Cohen, M. Cowan, S. Datwani, V. L. Davidson, J. Defever, B. Eaton, R. Ellson, Y. Feng, L. P. Ghislain, J. M. Glownia, G. Han, J. Hattne, J. Hellmich, A. H??roux, M. Ibrahim, J. Kern, A. Kuczewski, H. T. Lemke, P. Liu, L. Majlof, W. M. McClintock, S. Myers, S. Nelsen, J. Olechno, A. M. Orville, N. K. Sauter, A. S. Soares, S. M. Soltis, H. Song, R. G. Stearns, R. Tran, Y. Tsai, M. Uervirojnangkoorn, C. M. Wilmot, V. Yachandra, J. Yano, E. T. Yukl, D. Zhu and A. Zouni, *Structure*, 2016, **24**, 631–640.

11 A. Ishchenko, V. Cherezov and W. Liu, *J. Vis. Exp.*, 2016, 1–8.

12 F. D. Fuller, S. Gul, R. Chatterjee, E. S. Burgie, I. D. Young, H. Lebrette, V. Srinivas, A. S. Brewster, T. Michels-Clark, J. A. Clinger, B. Andi, M. Ibrahim, E. Pastor, C. de Lichtenberg, R. Hussein, C. J. Pollock, M. Zhang, C. A. Stan, T. Kroll, T. Fransson, C. Weninger, M. Kubin, P. Aller, L. Lassalle, P. Bräuer, M. D. Miller, M. Amin, S. Koroidov, C. G. Roessler, M. Allaire, R. G. Sierra, P. T. Docker, J. M. Glownia, S. Nelson, J. E. Koglin, D. Zhu, M. Chollet, S. Song, H. Lemke, M. Liang, D. Sokaras, R. Alonso-Mori, A. Zouni, J. Messinger, U. Bergmann, A. K. Boal, J. M. Bollinger, C. Krebs, M. Högbom, G. N. Phillips, R. D. Vierstra, N. K. Sauter, A. M. Orville, J. Kern, V. K. Yachandra and J. Yano, *Nat. Methods*, 2017, **14**, 443–449.

13 D. A. Sherrell, A. J. Foster, L. Hudson, B. Nutter, J. O'Hea, S. Nelson, O. Par??-Labrosse, S. Oghbaey, R. J. D. Miller and R. L. Owen, *J. Synchrotron Radiat.*, 2015, **22**, 1372–1378.

14 J. S. Fraser, H. van den Bedem, A. J. Samelson, P. T. Lang, J. M. Holton, N. Echols and T. Alber, *Proc. Natl. Acad. Sci.*, 2011, **108**, 16247–16252.

15 D. Axford, R. L. Owen, J. Aishima, J. Foadi, A. W. Morgan, J. I. Robinson, J. E. Nettleship, R. J. Owens, I. Moraes, E. E. Fry, J. M. Grimes, K. Harlos, A. Kotecha, J. Ren, G. Sutton, T. S. Walter, D. I. Stuart and G. Evans, *Acta Crystallogr. Sect. D Biol. Crystallogr.*, 2012, **68**, 592–600.

16 J. Friend, L. Yeo, M. Tan and R. Shilton, *Proc. - IEEE Ultrason. Symp.*, 2008, **14910**, 930–933.

17 F. Guo, W. Zhou, P. Li, Z. Mao, N. H. Yennawar, J. B. French and T. J. Huang, *Small*, 2015, **11**, 2733–7.

18 S. S. Sadhal, *Lab Chip*, 2012, **12**, 2600–11.

19 M. Gedge and M. Hill, *Lab Chip*, 2012, **12**, 2998–3007.

20 J. Sanchez-Weatherby, M. W. Bowler, J. Huet, A. Gobbo, F. Felisaz, B. Lavault, R. Moya, J. Kadlec, R. B. G. Ravelli and F. Cipriani, *Acta Crystallogr. Sect. D Biol. Crystallogr.*, 2009, **65**, 1237–1246.

21 A. S. Brewster, D. G. Waterman, J. M. Parkhurst, R. J. Gildea, T. M. Michels---clark, I. D. Young, H. J. Bernstein, G. Winter, G. Evans and N. K. Sauter, *Comput. Crystallogr. Newsl.*, 2016, **7**, 32–53.

22 M. Uervirojnangkoorn, O. B. Zeldin, A. Y. Lyubimov, J. Hattne, A. S. Brewster, N. K. Sauter, A. T. Brunger and W. I. Weis, *Elife*, 2015, **4**, 1–29.

23 S. Tsujino and T. Tomizaki, *Nat. Publ. Gr.*, 2016, 1–9.

24 S. L. Perry, S. Guha, A. S. Pawate, A. Bhaskarla, V. Agarwal, S. K. Nair and P. J. a Kenis, *Lab Chip*, 2013, **13**, 3183–7.

25 M. Maeki, H. Yamaguchi, M. Tokeshi and M. Miyazaki, *Anal. Sci.*, 2016, **32**, 3–9.

26 R. J. Gildea, D. G. Waterman, J. M. Parkhurst, D. Axford, G. Sutton, D. I. Stuart, N. K. Sauter, G. Evans and G. Winter, *Acta Crystallogr. Sect. D Biol. Crystallogr.*, 2014, **70**, 2652–2666.

27 O. B. Zeldin, M. Gerstel and E. F. Garman, *J. Appl. Crystallogr.*, 2013, **46**, 1225–1230.

28 R. J. Southworth-Davies, M. A. Medina, I. Carmichael and E. F. Garman, *Structure*, 2007, **15**, 1531–1541.